Hindawi
Mathematical Problems in Engineering
Volume 2021, Article ID 6692068, 14 pages
https://doi.org/10.1155/2021/6692068

Research Article

An Adaptability Analysis of the Space-Vehicle Traffic State Estimation Model for Sparsely Distributed Observation Environment

Han Yang[1] **and Qing Yu**[2]

[1]*Research Institute of Highway Ministry of Transport, Xitucheng Road, Beijing 100088, China*
[2]*The Key Laboratory of Road and Traffic Engineering of the Ministry of Education School of Transportation Engineering, Tongji University, Shanghai, China*

Correspondence should be addressed to Qing Yu; 1810514@tongji.edu.cn

Received 4 November 2020; Revised 11 December 2020; Accepted 13 January 2021; Published 22 January 2021

Academic Editor: Constantine Michailides

The autonomous driving has shown its enormous potential to become the new generation of transportation in the last decade. Based on the automated technology, vehicles can drive in a new form, vehicle platoon, which can significantly increase the efficiency of the road system and save road resources. The space-vehicle traffic state estimation model has shown its benefits in modeling autonomous vehicle platoon in nonpipeline corridors with on- and off-ramps in ideal observation environment. However, in the current initial stage of automated connected vehicles' application, the observation environment is quite imperfect. Limited by financial and investment, traffic flow observation equipment is sparsely distributed on the road. How to adapt to the sparse observer layout is a critical issue in the current application of the space-time traffic state estimation, which is originally designed for the autonomous transportation. Therefore, this manuscript overviews the observation environment in practice and summarizes three key observation problems. This article designs 22 numerical experiments focusing on the three key issues and implements the space-time estimation model in different observation scenarios. Finally, the observation environment adaptability is analyzed in detail based on the experiment results. It is found that the accuracy of the estimation results can be improved with the highest efficiency under the premise of limited equipment input by reducing the observation interval to 1000 m and increasing the density of the observer to 1/km. For the road sections with relatively homogeneous traffic conditions, the layout of observation equipment can be relatively reduced to save the investment input. Also, the maintenance of observation equipment for the ramp with larger flow can be slowed down appropriately in limited equipment investment. This manuscript is of great practical significance to the popularization and application of connected automatic transportation.

1. Introduction

Autonomous driving has obtained abundant attractions in the last decade. Road automated driving as a new generation of information technology and the integration of the transport industry's development has become a new round of global scientific and technological innovation and industrial transformation. This technology will promote the continuous upgrading of the field of road traffic. At present, the government, enterprises, and investors all take this as the goal and direction to accelerate automated driving around the world [1–3].

In the ideal application scenario of autonomous driving, the next generation of sustainable urban development requires a new wave of infrastructure construction. However, in the early development stage of autonomous driving, due to financial and investment constraints, existing infrastructure needs to adapt to the application and promotion of autonomous driving. Therefore, we need to propose a traffic model that is not only applicable to the operation

mechanism of automatic driving but also can adapt to the existing observation infrastructure.

In the field of traffic flow modeling for connected automatic vehicles, the space-vehicle traffic flow model (referred to as "N-X traffic flow model") with vehicles as the research object has been proposed since 2007 [4, 5]. Besides the traditional space-time model (referred to as "X-T traffic flow model") based on space (referred to as "X") and time (referred to as "T") dimension [6–9], the traffic flow can also be described in vehicle (referred to as "N") dimension. In the X-T model, traffic flow can be described as the traffic character variables such as flow rate and speed varying with time index. Similarly, In the N-T model, traffic flow can be described in a different form: traffic character variables such as headway and pace which are varying with the vehicle index. In the X-T model, the time index can be integrated into 10 seconds or 5 minutes. Similarly, the vehicle index in the N-X model can also be integrated into a vehicle packet with 5 vehicles or 10 vehicles as well. The N-X model has attracted many researchers' interest and has shown its advantages in modeling vehicle platoon, which is the essential form of connected automatic traffic flow. In other words, the N-X model has shown its enormous potentials in the connected automatic transportation system. In 2014, Jin proposed the traffic state estimation framework based on the N-X traffic flow model (referred to as the N-X traffic state estimation model) for a pipeline corridor without inflow and outflow [10]. In 2019, Yang proposed an N-X traffic state estimation model adding the node model [11]. Then, this model can be applied into nonpipeline corridors with on- and off-ramps. Then, in 2019, Yang proposed a revised nonpipeline N-X traffic state estimation model by reducing the node assumption [12]. The proposed N-X traffic state estimation model has shown its adaptability in fixed-point vehicle matching detection environment. It is worth noting that the adaptability is mainly verified in the ideal observation environment. In the proposed model, the ideal observation environment refers to the relatively dense layout of traffic flow observers.

In recent years, with the reduced cost and wide use of data acquisition equipment, high quality, reliable data, and robust models are essential to the development of the intelligent transportation system, and transportation data mining based on big geospatial data has become a research hotspot and earns a lot of attention [13–15]. These emerged big data-based technologies have been proved as central to the development of transportation operation and management [16, 17].

With the rapid development in automobile manufacturing, industrial investment, and financing in the last two years, connected automatic vehicles are gradually finishing the theoretical verification and starting to enter the practical road environment. However, the development of the data environment of automatic driving is still in its infancy, and the infrastructure cannot generate high quality and reliable data to support the application of new big data mining technology. In other words, compared with the dense detector layout environment, the sparse layout detection environment will be widely applied in practical applications.

Therefore, for the initial application and promotion of connected automatic vehicles, it is very important to study the adaptability of the N-X traffic state estimation model in the practical imperfect detection environment with sparse detector layout, which has high potential to support the development of the next-generation intelligent transportation system.

Therefore, in this paper, the adaptability of the N-X traffic state estimation model is analyzed in detail in view of the practical imperfect detector layout environment, which is of great practical significance to the popularization and application of connected automatic transportation. This manuscript first analyzes the existing problems in the practical observation environment. Secondly, the observation infrastructure environment is designed and simulated based on the urban channel. The ability to adapt to the actual observation infrastructure environment is discussed from three aspects: trunk road observation equipment damage, trunk road observation interval distance, and ramp observation equipment missing. Finally, this article puts forward the design and planning suggestion of the observation infrastructure's layout in connected automated vehicle scenario.

2. Overview of Imperfect Observation Environment

Automatic vehicle license plate recognition (ALPR) is one of the important components in modern intelligent transportation systems [18]. ALPR technology can detect vehicles on the monitored road surface through roadside fixed observation equipment and automatically extract vehicle license plate information (including Chinese characters, English letters, Arabic numerals, and plate colors) for processing. At present, this technology has been widely used in highway vehicle management [19]. In practice, affected by natural conditions, financial investment, operation, and maintenance, the actual observation environment of ALPR is often "imperfect." For example, the damage of the equipment on main roads and ramps often occurs because of the maintenance. Also, the limit of financial investment and natural conditions often lead to the too wide layout intervals of the equipment on main roads.

Problem 1. Damaged main road observer

Affected by factors such as equipment operation and maintenance, the vehicle license plate recognition observer deployed on arterial roads is often damaged. The damaged observation equipment cannot transmit effective arterial road observation data, which will result in a lack of observation space for arterial road. Figure 1 shows the distribution of vehicle license plate recognition observers in Shenzhen, among which about 10% of vehicle license plate observers are damaged.

Problem 2. Different observation interval on arterial road

The arterial road observation interval size refers to the spatial distance between adjacent observers on the arterial road. The interval of the main road observation interval will be affected by factors such as financial investment and equipment layout environment. In addition, the granularity of the observation interval on arterial roads is often various

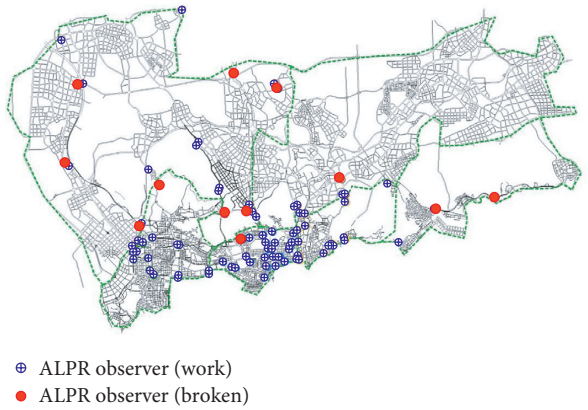

Figure 1: Layout and distribution of vehicle license plate recognition observation equipment in Shenzhen

for different observation scenarios such as expressways in central areas, expressways in suburbs, and expressways outside cities. Taking Shanghai as an example, the VLPR observation interval within the inner ring expressway is about 300m–500 m, on the middle ring expressway is about 1 km, and on the outer city expressway can reach 2 km or more.

Problem 3. Ramp observer missing

The ALPR observation equipment is also deployed on the up-ramp and the down-ramp to effectively detect the information of vehicles entering and exiting the arterial road. However, because the license plate recognition system is more inclined to recognize vehicles entering the main road, the observation equipment located on the off-ramp is often missing. In addition, with the deepening of urbanization, urban road networks are highly dense, which leads to the numerous ramps. Then, in practice, it is quite normal to cut down the ramp observation equipment to save investment. For example, in Shanghai's ALPR system, there is no observation equipment on off-ramps, and about 70% of the on-ramps do not install observation equipment.

3. Methodology

3.1. N-X State Process Model. The classic traffic state estimation framework includes two key components: a state process model and a measurement model [20–26]. Based on the proposed travel time transmission model, the state process model for the nonpipeline N-X Kalman filter framework is formulated as

$$\begin{aligned} T_i(n+1) &= T_i(n) + \Delta n_i \left(p_{i+1}(n) - p_i(n)\right) \\ &\quad + \Delta n_i \left(\frac{p_{i+1}(n)^2 \left(\left(1/p_i^r(n)\right) - \left(1/p_i^s(n)\right)\right)}{1 - p_{i+1}(n)\left(\left(1/p_i^r(n)\right) - \left(1/p_i^s(n)\right)\right)} \right) \\ &\quad + \zeta_i(n), \end{aligned} \tag{1}$$

$$p_i(n) = \max\left\{ p^*, \frac{1}{C_i}, \frac{h_{\text{jam},i}\left(T_i(n) - T_{\text{free},i}\right)}{\Delta x_i} + \frac{1}{C_i} \right\}, \tag{2}$$

where $\zeta_i(n)$ denotes the state noise in the estimation. Travel time $T_i(n)$ is the state variable; $p_i(n)$ is a function of $T_i(n)$ based on equation (2) from the fundamental diagram, and $p_i^r(n)$ and $p_i^s(n)$ are system external input variables. System parameters include the capacity C_i, jam distance headway $h_{\text{jam},i}$, and free-flow travel time $T_{\text{free},x}$ for each segment i. System boundary variables include $p_1(n)$ and $p_{M+1}(n)$. In this paper, for the free-flow regime in the N-X fundamental diagram, p^* is defined as follows:

$$p^* = \max\left\{ p_i(n-1), \frac{1}{C_i} \right\}. \tag{3}$$

3.2. N-X Measurement Model. In practice, travel time cannot be fully observed because of the limited penetration of probe vehicle. Thus, we formulate the N-X measurement model as

$$\widehat{T}_i(n) = T_i(n) + \xi_i(n) = \Delta \mathrm{x} \cdot \tau_{\mathrm{x}}(\mathrm{n}) + v_x^{\tau}(\mathrm{n}), \tag{4}$$

where $\widehat{T}_i(n)$ denotes the estimated measurement of travel time $T_i(n)$ and $\xi_i(n)$ is the measurement noise.

3.3. State-Space Model. The state-space representation for the N-X traffic state estimation framework is given as follows:

$$\begin{aligned} T(n) &= F\left(T(n-1), b(n-1), u(n-1), \alpha(n-1), \zeta(n-1)\right), \\ \widehat{T}(n) &= H\left(T(n), \xi(n)\right), \end{aligned} \tag{5}$$

where

$$\begin{aligned} \begin{bmatrix} T_1(n) \\ T_2(n) \\ \cdots \\ T_M(n) \end{bmatrix} &= \begin{bmatrix} f\left(T_1(n-1), b_1(n-1), u_1(n-1), \alpha_1(n-1),\right) \\ f\left(T_2(n-1), b_2(n-1), u_2(n-1), \alpha_2(n-1),\right) \\ \cdots \\ f\left(T_M(n-1), b_M(n-1, X), u_M(n-1, X), \alpha_M(n-1)\right) \end{bmatrix} + \begin{bmatrix} \zeta_1(n-1) \\ \zeta_2(n-1) \\ \cdots \\ \zeta_M(n-1) \end{bmatrix}, \\ \widehat{T}(n) &= \begin{bmatrix} 1 & 0 & \cdots & 0 \\ 0 & 1 & \cdots & 0 \\ \vdots & \vdots & \ddots & \vdots \\ 0 & 0 & \cdots & 1 \end{bmatrix} \cdot T(n) + \xi(n). \end{aligned} \tag{6}$$

F and H are the vector functions based on equation (1)–(4). Vectors T, b, u, α, ζ, $\widehat{T}$, and ξ are system state variable, boundary variable, control input variable, parameter, process noise, system observation variable, and measurement noise, respectively. These vectors are defined as follows:

$$\begin{aligned}
T(n) &= \left[\, T_1(n) \;\; T_2(n) \;\; \ldots \;\; T_M(n) \,\right]^T, \\
b(n) &= \left[\, p_1(n) \;\; p_{M+1}(n) \,\right]^T, \\
u(n) &= \left[\, p_1^r(n) \;\; p_1^s(n) \;\; \ldots \;\; p_M^r(n) \;\; p_M^s(n) \,\right], \\
\alpha(n) &= \begin{bmatrix} h_{\text{jam},1}(n) & \tau_{\text{free},1}(n) & C_1(n) \\ \vdots & \vdots & \vdots \\ h_{\text{jam},M}(n) & \tau_{\text{free},M}(n) & C_M(n) \end{bmatrix}, \\
\zeta(n) &= \left[\, \zeta_1(n) \;\; \zeta_2(n) \;\; \ldots \;\; \zeta_M(n) \,\right]^T, \\
\widehat{T}(n) &= \left[\, \widehat{T}_1(n) \;\; \widehat{T}_2(n) \;\; \ldots \;\; \widehat{T}_M(n) \,\right]^T, \\
\xi(n) &= \left[\, \xi_1(n) \;\; \xi_2(n) \;\; \ldots \;\; \xi_M(n) \,\right]^T.
\end{aligned} \tag{7}$$

3.4. Unscented Kalman Filter Configuration. Because state process model equation (1) is nonlinear, unscented Kalman filter (UKF) is applied to estimate the traffic state. The UKF is an effective filter method for nonlinear systems, avoiding the linear approximation error and Jacobian matrix calculation. The UKF relies mainly on unscented transform (UT) to process the mean and covariance transition in a nonlinear system [27, 28].

3.5. Performance Evaluation. To illustrate the estimation result, the traffic state travel time $T_i(n)$ in the N-X model is converted to travel speed $u_i(n)$. Furthermore, the N-X result recorded in the vehicle dimension is converted into the time dimension $u_i(t)$ via the N-X interpolation method [21]. The method tracks the link entry time of each flow packet and conducts linear interpolation of the traffic states.

The performances of the results are evaluated by the following performance indexes: the root mean squared error (RMSE), mean absolute error (MAE), and mean absolute percentage error (MAPE). They are defined as follows:

$$\begin{aligned}
\text{RMSE}_i &= \sqrt{\frac{1}{\Theta}\sum_{t=1}^{t=\Theta}\left(u_i^{GT}(t) - \widetilde{u}_i(t)\right)^2}, \\
\text{MAE}_i &= \frac{1}{\Theta}\sum_{t=1}^{t=\Theta} u_i^{GT}(t) - \widetilde{u}_i(t), \\
\text{MAPE}_i &= \frac{1}{\Theta}\sum_{t=1}^{t=\Theta}\left|\frac{u_i^{GT}(t) - \widetilde{u}_i(t)}{u_i(t)}\right| \times 100\%,
\end{aligned} \tag{8}$$

where $i = 1, \ldots, \text{M}$. Θ is the total number of time index during the estimation period:

$$\Theta = 3.5 \times \frac{3600}{\Delta t}. \tag{9}$$

M is the total number of segments in the corridor. $u_i^{GT}(t)$ and $\widetilde{u}_i(t)$ are the ground truth state and estimated state of segment i at timestamp t, respectively.

4. Design of Numerical Experiment

4.1. Simulation Model and Parameters. The proposed N-X estimation model is evaluated through the VISSIM simulation model, which is calibrated by field loop data. VISSIM simulation allows for flexibility in generating vehicle-based paired detector data, along with high-resolution ground truth data for evaluating the congestion patterns. The VISSIM simulation model is established and calibrated by field loop detector data from IH-894 in Milwaukee, Wisconsin, during the morning peak hours from 5 : 30 am to 9 : 30 am [29]. The simulated area is a 4-mile segment of a nonpipeline freeway corridor with five on-ramps and three off-ramps, as shown in Figure 2. The nonpipeline freeway includes a significant bottleneck, which can be used to further analyze the accuracy of the model in the congestion pattern.

The entire corridor is divided into 12 segments with the same length of 500 m. Propagation packet size Δn is set as 50 vehicles for all the segments with (or without) freeway ramps. Uniform traffic parameters are assumed across the entire corridor to simplify the calculation. Then, C, k_{jam}, and u_{free} are 7,200 veh/h, 500 veh/km, and 100 km/h, respectively. In the estimation process, the system and observation noise are assumed to be 1% of the average traffic state value and observation value, respectively. The assumption for traffic system state and observation noise is as the same as the noise assumption in [21]. The uncertainty terms, R and Q, are defined as $0.5 * I(M)$, where $I(M)$ is a unit matrix with M dimensions.

4.2. Observation Environment. This paper designs the numerical observation environment according to the actual observation situation of ALPR. The designed scene is a partial passage of Highway 894 (I-894) in Milwaukee, Wisconsin, USA, with a total length of 6.5 km. The designed scene channel contains 13 sequentially numbered cells, and Cell 1 and Cell 13 are the boundary cells of the channel. License plate observers are set up between each adjacent channel, as the blue rectangle identified in Figure 3, numbered A0, A1, A2, ..., A11, A12, and A13. Through the vehicle license plate observers placed at the boundary position at both ends of the cell, the time information of the vehicle passing the cell boundary can be recorded, and the travel time of the vehicle through the cell can be obtained. Observers A0, A1, A12, and A13 are set as the boundary observers of the channel to obtain the travel time of the channel boundary cell (Cell 1 and Cell 12). These observers' layout conditions remain unchanged and the passing time information of all passing vehicles can be obtained. Observers A2, A3, ..., A10, and A11 are experimentally designed ALPR observation equipment. In addition, the green line segments identified in the figure are the license plate recognition

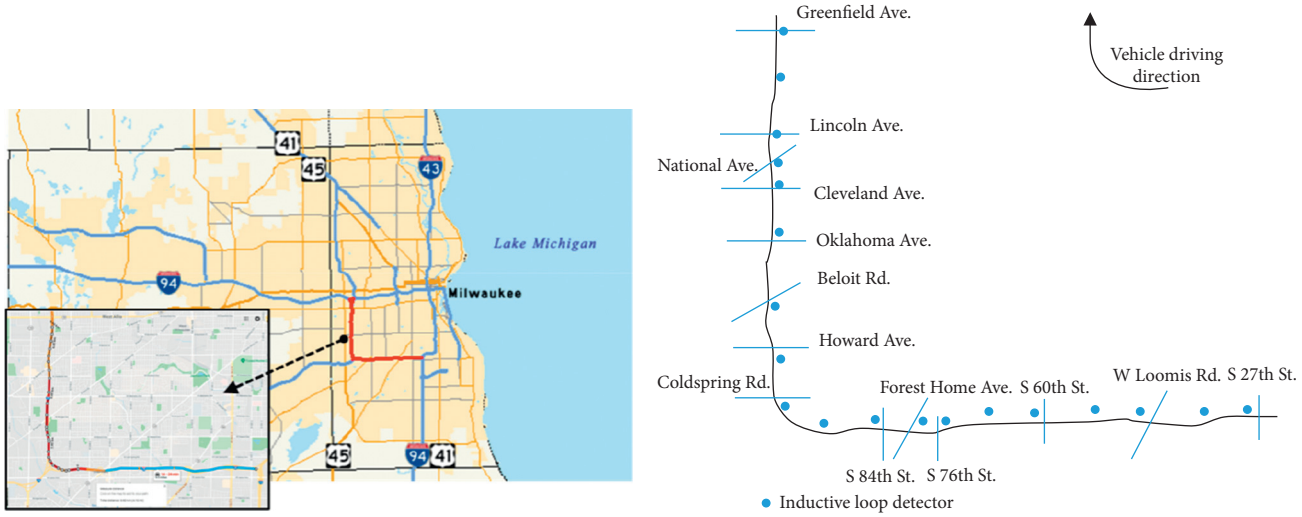

Figure 2: Detail of IH-894 in Milwaukee.

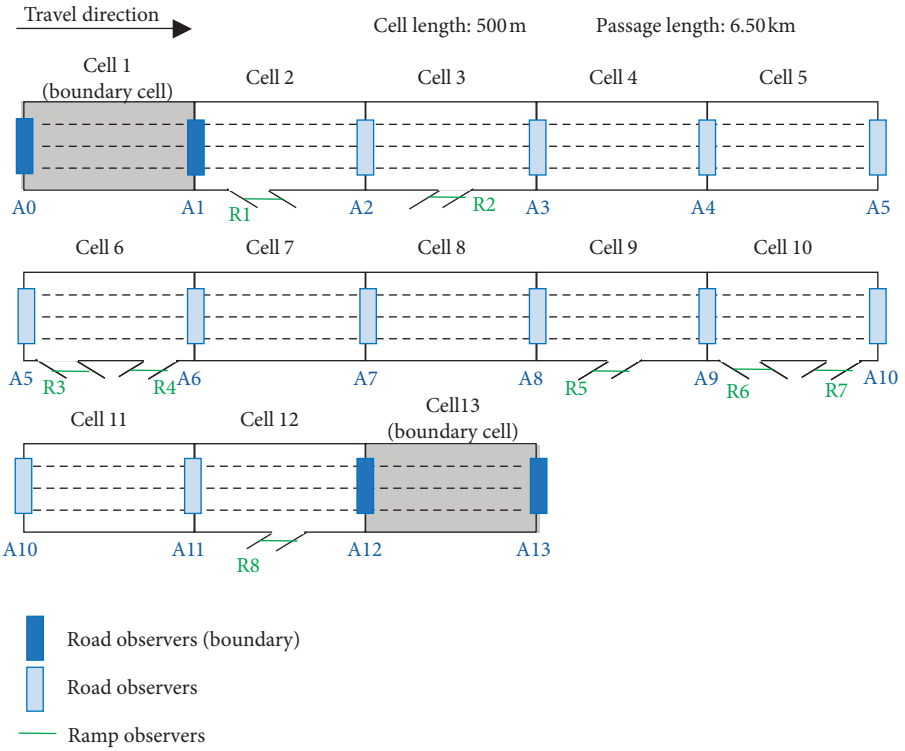

Figure 3: Simulation of observation environment.

observers placed on the up- and down-ramps, which are numbered as R1, R2, ..., R7, and R8 in sequence. This paper will design different observation equipment layout based on different experimental observation scenarios.

4.3. Observation Scenarios

Scenario 1. Damaged arterial road observer

The damage rate of the arterial road observers in the actual observation environment is about 10%. Therefore, for the 10 trunk road observers designed in the experimental scene, we assume that there is a damaged observer in the channel. According to the 10 trunk road observers laid out in the passage, 10 groups of cases are designed in this section, corresponding to damaged observers A2, A3, ..., A10, and A11, respectively, as shown in Table 1. For example, in CASE A-2, observer A3 is damaged, as shown in Figure 4. Then, red observer A3 is the damage observer, and the travel time of the vehicle in Cell 3 and Cell 4 cannot be obtained directly. In this case, only the travel time of the vehicle passing through Cell 3 and Cell 4 can be obtained. In addition, because Cell 3 contains an up-ramp, the number of vehicles passing through Cell 4 is higher than that passing through

Table 1: Scenario design of arterial road observer damaged.

Scenario	Damaged observer	Upstream cell	Downstream cell
CASE A-1	A2	Cell 2	Cell 3
CASE A-2	A3	Cell 3	Cell 4
CASE A-3	A4	Cell 4	Cell 5
CASE A-4	A5	Cell 5	Cell 6
CASE A-5	A6	Cell 6	Cell 7
CASE A-6	A7	Cell 7	Cell 8
CASE A-7	A8	Cell 8	Cell 9
CASE A-8	A9	Cell 9	Cell 10
CASE A-9	A10	Cell 10	Cell 11
CASE A-10	A11	Cell 11	Cell 12

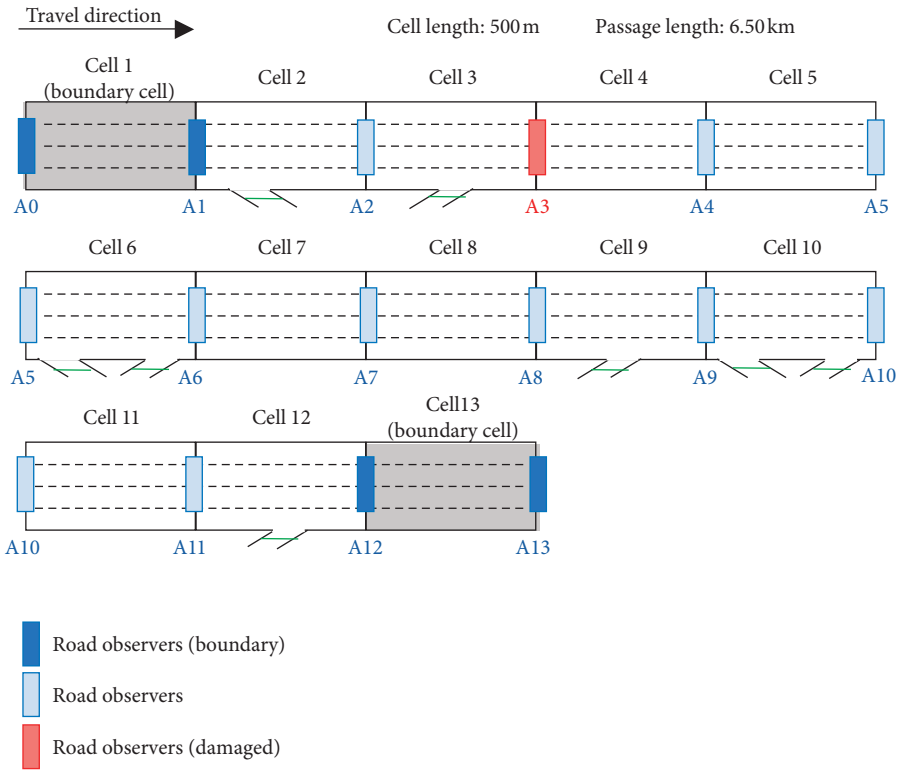

Figure 4: Example of scenario 1 (CASE A-2).

Cell 3. In other words, several vehicles' channel entering time cannot be found in the ALPR system. Then, according to the travel time calculation principle of license plate recognition and matching, only a part of vehicles' travel time information in Cell 4 can be obtained.

Scenario 2. Different observation intervals on arterial road

The granularity of arterial road observation interval refers to the spatial distance between adjacent observers on the arterial road. Because of the limitation of funds and technology, the distance between adjacent trunk road observers in the actual observation environment is between 500 m and 2 km. For the experimental channel, four arterial road observers' interval granularities are designed: 500 m, 1000 m, 1500 m, and 2000 m, as shown in Table 2. For example, in CASE B-2, the observation interval distance is set as 1000 m as, as shown in Figure 5. Limited by the designed observation interval granularity, the travel time of the vehicle in Cell 2 and Cell 3 cannot be obtained directly, and only the travel time of the vehicle passing through Cell 2 and Cell 3 can be obtained. In addition, since Cell 2 contains a down-ramp and Cell 3 contains an up-ramp, only a part of vehicles' travel time can be recorded. According to the travel time calculation principle, the ALPR system can obtain the travel time information of vehicles passing through observers A1 and A3 successively and cannot record the information of vehicles leaving the Cell 2 through off-ramp or entering the Cell 3 through on-ramp.

Scenario 3. Ramp observer missing

Due to the limitations of funds, technology framework, and functional requirements of the ALPR system, license

Table 2: Scenario design of arterial road observation interval granularity.

Scenario	Observation interval (m)	Division of observation section
CASE B-1	500	[Cell 2]; [Cell 3];. . .; [Cell 11]; [Cell 12]
CASE B-2	1000	[Cell 2-Cell 3]; [Cell 4-Cell 5]; [Cell 6-Cell 7]; [Cell 8-Cell 9]; [Cell 10-Cell 11]; [Cell 12]
CASE B-3	1500	[Cell 2-Cell 3-Cell 4]; [Cell 5-Cell 6-Cell 7]; [Cell 8-Cell 9-Cell 10]; [Cell 11-Cell 12]
CASE B-4	2000	[Cell 2-Cell 3-Cell 4-Cell 5]; [Cell 6-Cell 7-Cell 8-Cell 9]; [Cell 10-Cell 11-Cell 12]

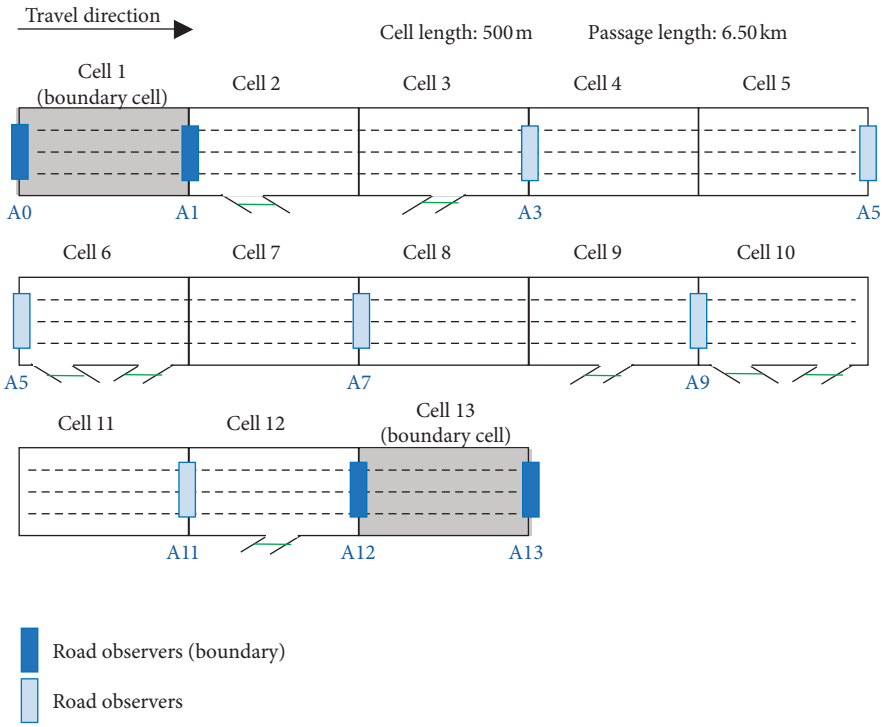

Figure 5: Example of scenario 2 (CASE B-2).

plate identification observer on-ramps are often missing in the actual observation environment. For example, the ALPR system in Shanghai does not install the corresponding observation equipment in the off-ramp part. However, when other observation data, such as inductive loop data, are used to supplement the observation function, there are often data mismatching problems in heterogeneous granularity, inconsistent mean variance, and inconsonant spatial and temporal range. Therefore, in the experimental channel, we design eight scenarios of missing ramp observation equipment, as shown in Table 3 and Figure 6. The detailed cell number, ramp observer number, ramp type, and average ramp flow were recorded, respectively, in the table.

5. Results and Analysis

The estimation results of N-X traffic state estimation framework in scenarios of different experimental observation scenes are shown in Figures 7–9. The estimation results are transformed from travel time into travel speed to make results easy to be understood. The result figures have two forms: estimated travel speed figures and estimation error figures. In the estimated travel speed figures, the dark blue areas represent free-flow situation of 110 km/h, and the dark red areas represent blocked flow situation of 10 km/h. Black outline draws the contour of space-time congestion area of 30 km/h, which is a congestion time and space area surrounded by 30 km/h boundary. The figure can show the spatial and temporal development process of the generation, spread, and dissipation of congestion in the case channel during the morning rush hour. In the estimation error figures, the blue area represents the estimated result which is higher than the actual situation. In this case, the travel speed is overestimated, and the congestion is underestimated. The red area represents the estimated result which is lower than the actual situation. In this case, travel speed is underestimated, and congestion is overestimated. The green area represents the estimation error which is relatively close to 0. In this case, the estimated result is very close to the actual situation.

5.1. Adaptability Analysis of Damaged Arterial Road Observer. The estimation results of N-X traffic state estimation framework in scenarios of different damaged arterial road observers are shown in Figure 10 and Figure 8. It is found that the damage of the trunk road observer has a small impact on the estimation results of congestion status, but an

Table 3: Scenario design of ramp observer missing.

Scenario	Cell without ramp observer	Ramp observer missing	Ramp type	Traffic flow on-ramp (veh/h)
CASE C-1	Cell 2	R1	Off-ramp	972.14
CASE C-2	Cell 3	R2	On-ramp	1566.55
CASE C-3	Cell 6	R3	Off-ramp	218.75
CASE C-4	Cell 6	R4	On-ramp	332.09
CASE C-5	Cell 9	R5	On-ramp	481.12
CASE C-6	Cell 10	R6	Off-ramp	261.91
CASE C-7	Cell 10	R7	On-ramp	337.77
CASE C-8	Cell 12	R8	On-ramp	458.70

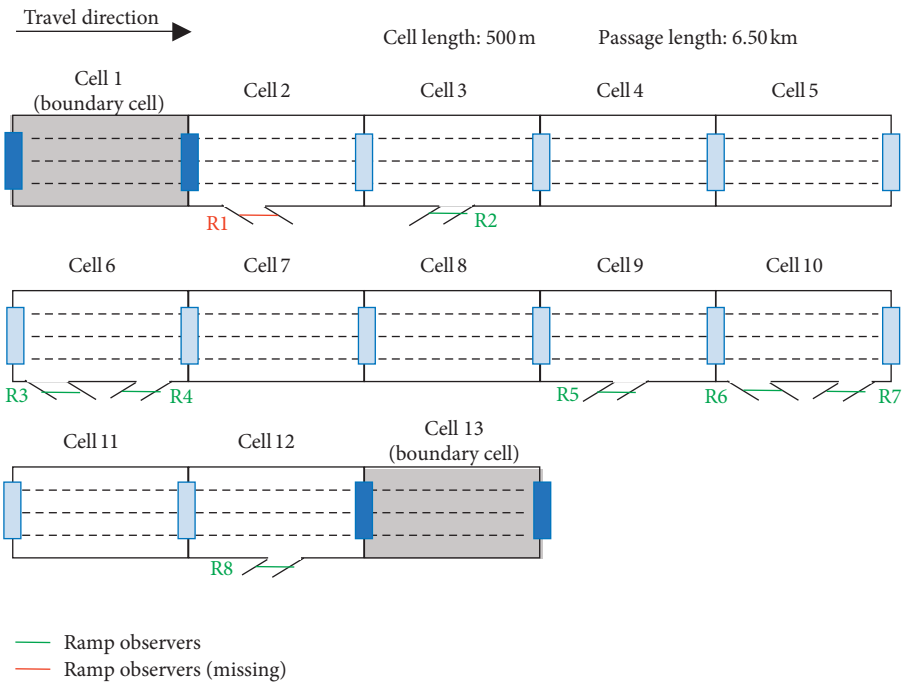

Figure 6: Example of scenario 3 (CASE C-1).

obvious impact on the estimation results of free-flow status. In addition, the damage of the trunk road observer has a significant impact on the travel speed estimation results of adjacent cells on both sides of the damage observer. For example, in CASE A-4, trunk road observer A5 was damaged, and the adjacent Cells 5 and 6 on both sides of observer A5 could not be directly observed. In other words, the space position cannot be directly observed within the range of 2.0 km to 3.0 km. Then, it is found that the estimation error near the broken observation increases, while the estimation error in other functioning observation areas does not increase significantly.

5.2. Adaptability Analysis of Different Observation Intervals. The estimation results of different trunk road observations' distance interval are as shown in Table 4 and Figure 8. The trunk road observation interval size refers to the space distance between the adjacent road observers. The number of the trunk observers refers to the number of installed observations on the channel. The trunk road observer layout density refers to the arterial observer number on unit space length, which is equal to the number of arterial road observer divided by channel distance. It is found that the estimation error of the channel increases gradually with the increasing distance between the adjacent observers of the trunk road. In addition, the estimation error of free-flow condition increases significantly, while the estimation error of congestion condition changes relatively little. Compared with the scenario of the damaged trunk road observers, the effect of changing the granularity of the trunk road observation interval on the estimated results is significantly higher.

The estimation results vary with trunk road observers' distribution density and distance interval, which is shown in Figure 11. The blue curve is the change of RMSE, and the green curve is the change of MAPE. From the figure, with the increase of the trunk road observations' distance interval, the density of trunk road observations gradually decreases, RMSE and MAPE both gradually increase, and the accuracy of estimation model decreases gradually. There is an inflection point of RMSE and MAPE indices between 1000 m and 1500 m in the observation range and between 0.91/km

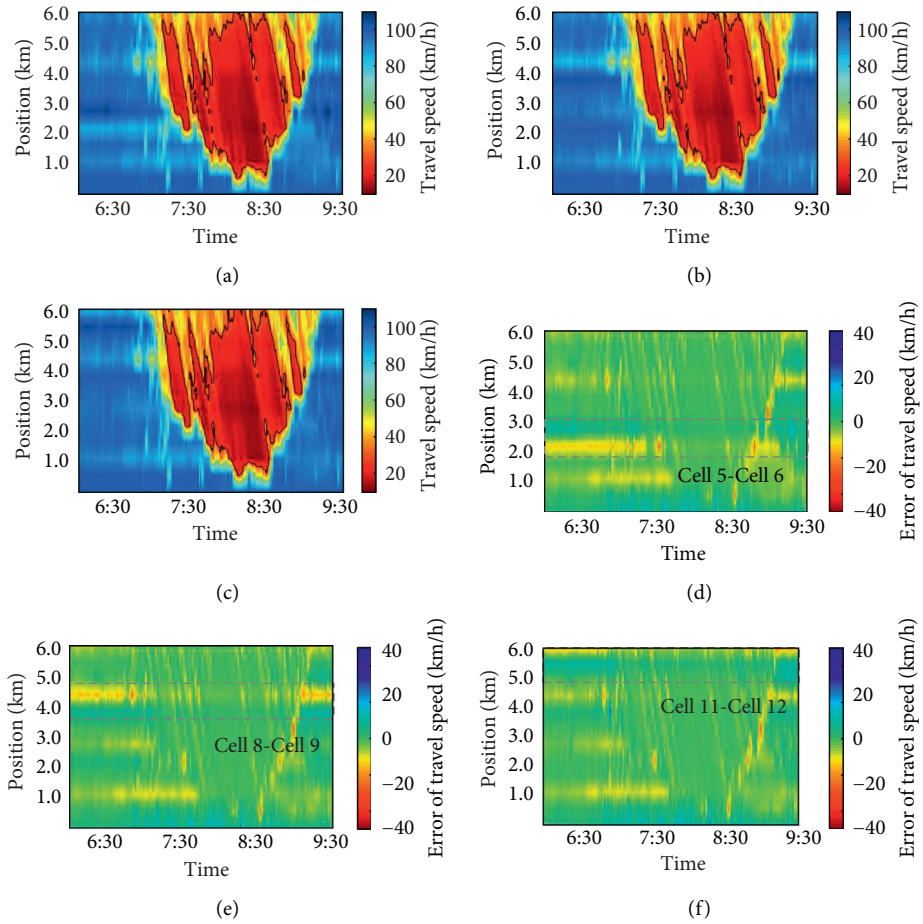

Figure 7: Result and error of scenario 1: (a) result of Case A-4, (b) result of Case A-7, (c) result of Case A-10, (d) error of Case A-4, (e) error of Case A-7, and (f) error of Case A-10

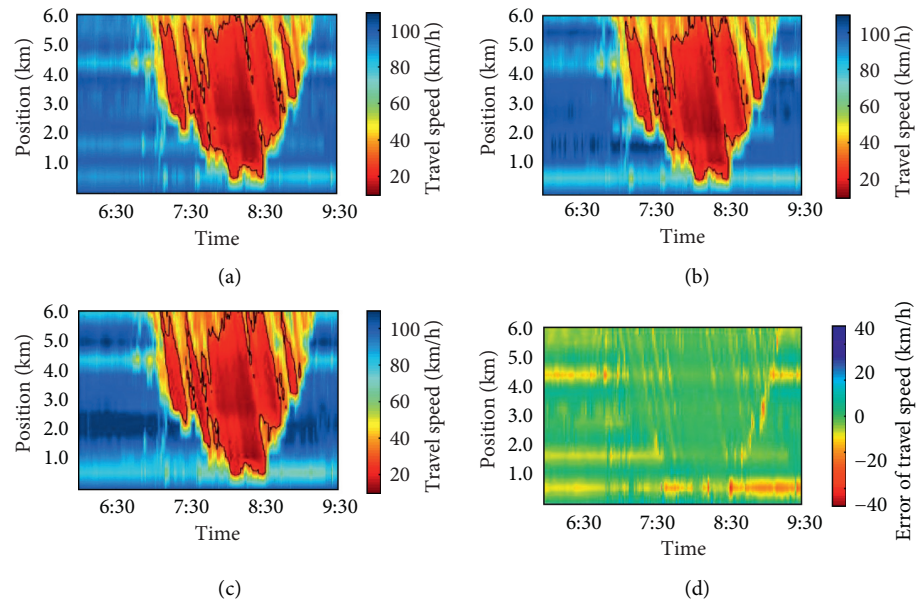

Figure 8: Continued.

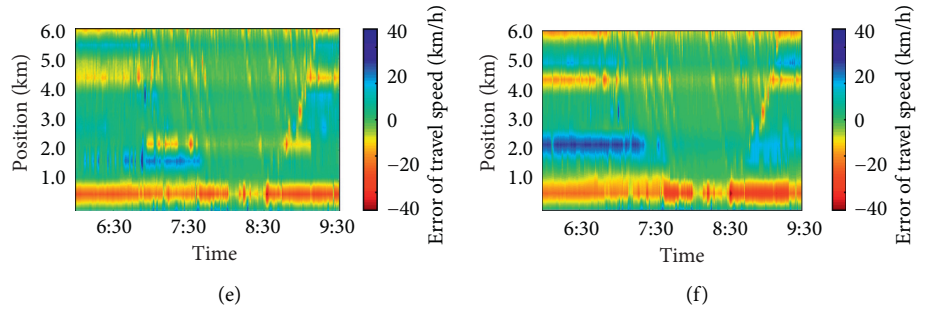

Figure 8: Result and error of scenario 2: (a) result of Case B-2, (b) result of Case B-3, (c) result of Case B-4, (d) error of Case B-2, (e) error of Case B-3, and (f) error of Case B-4.

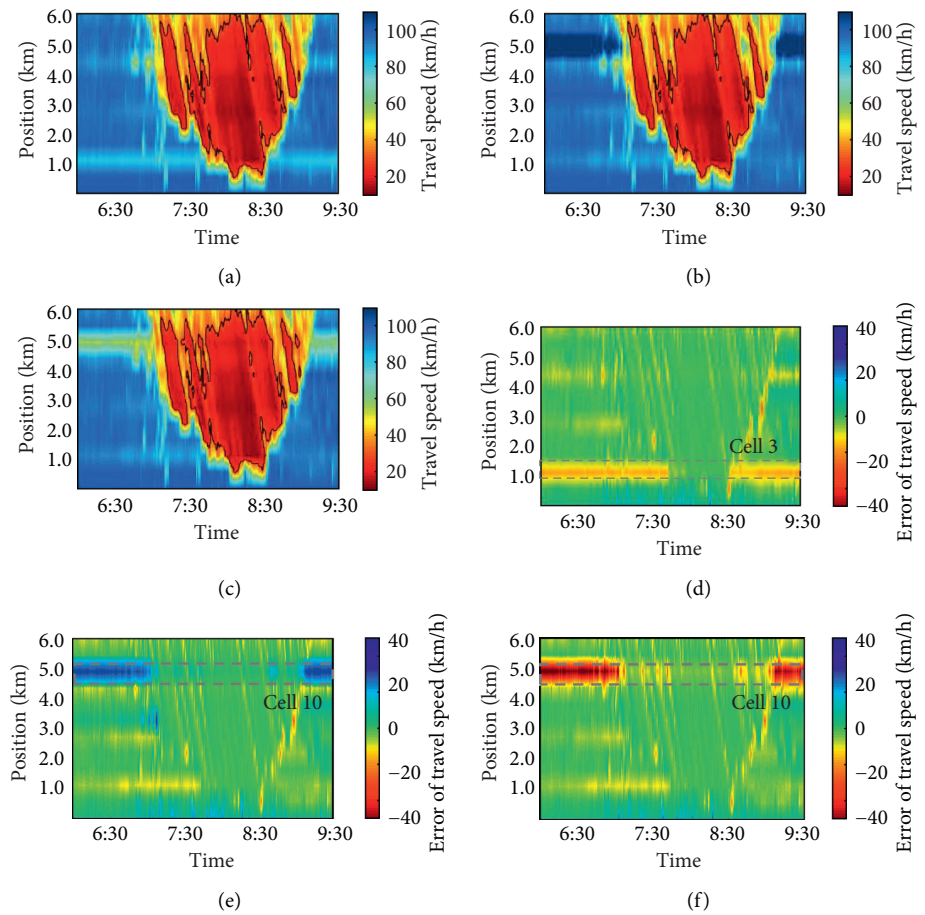

Figure 9: Result and error of scenario 3: (a) result of Case C-2, (b) result of Case C-6, (c) result of Case C-7, (d) error of Case C-2, (e) error of Case C-6, and (f) error of Case C-7.

and 1.27/km in the distribution density. Therefore, the accuracy of the estimation results can be improved with the highest efficiency by reducing the particle size of the observation interval to 1000 m and increasing the observer density to 1/km.

5.3. Adaptability Analysis of Missing Ramp Observers. The estimated results for different missing ramp observers are shown in Table 5 and Figure 10. It is found that the absence of ramp observation environment has a higher impact on the free-flow conditions but a smaller impact on the congestion conditions. In addition, for high inflow and outflow ramps (take CASE C-1 and CASE C-2 as examples), the absence of ramp observation equipment has a relatively small impact on the estimation results, while for low flow ramps, the absence of ramp observation equipment will significantly increase the estimation error and reduce the estimation accuracy.

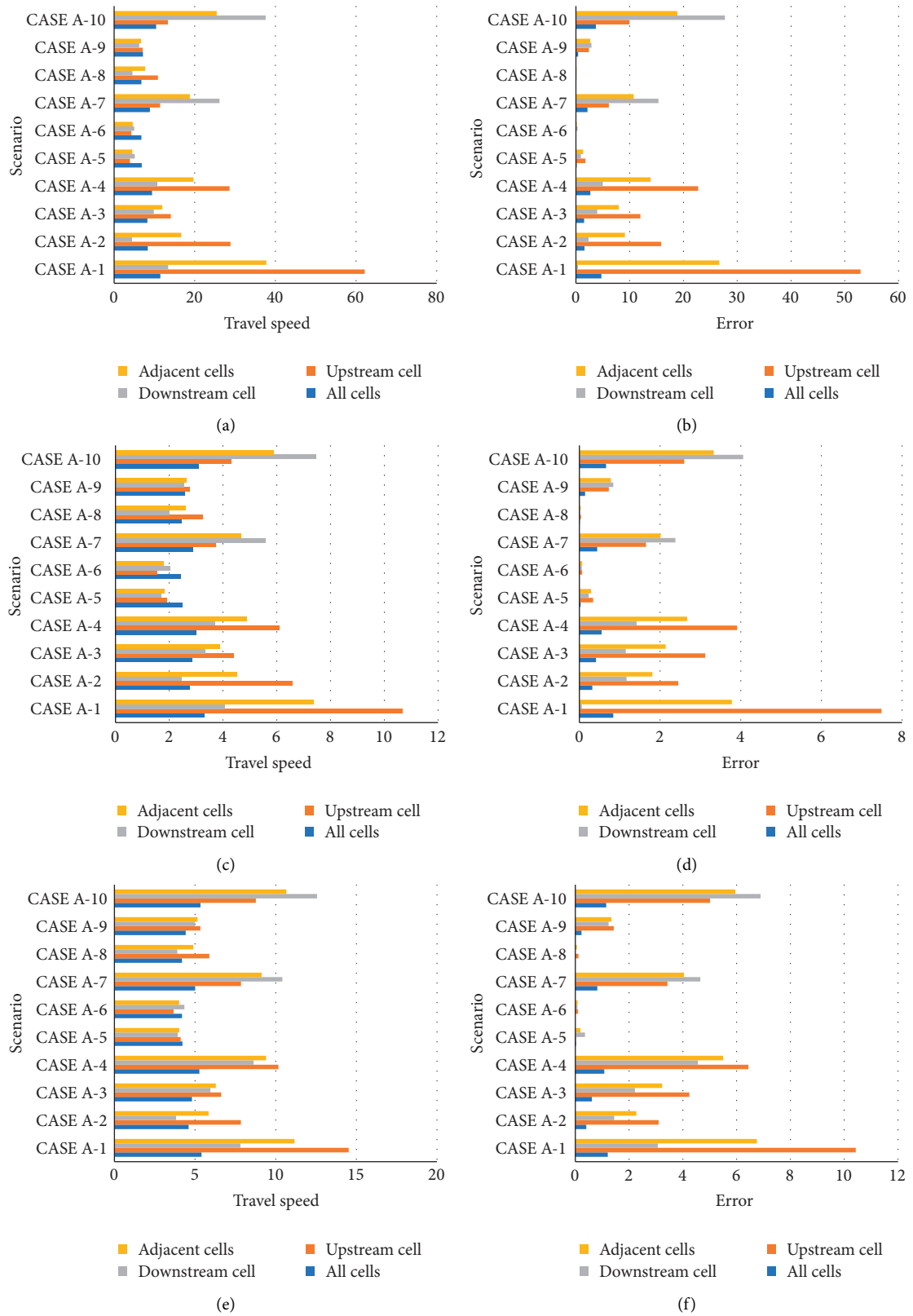

Figure 10: Result and error of scenario 1 under different evaluation methods: (a) result (RMSE: km/h), (b) result (RMSE: km/h), (c) result (MAE: km/h), (d) error (MAE: km/h), (e) result (MAPE: %), and (f) error (MAPE: %).

Table 4: Result of scenarios with different observation distance intervals.

Scenario	Observation interval (m)	Number of observers	Density of observers per km	RMSE (km/h)	MAE (km/h)	MAPE (%)
CASE B-1	500	12	2.18	6.73	2.46	4.19
CASE B-2	1000	7	1.27	15.96	3.99	6.80
CASE B-3	1500	5	0.91	35.89	5.80	9.57
CASE B-4	2000	4	0.73	49.21	6.77	10.85

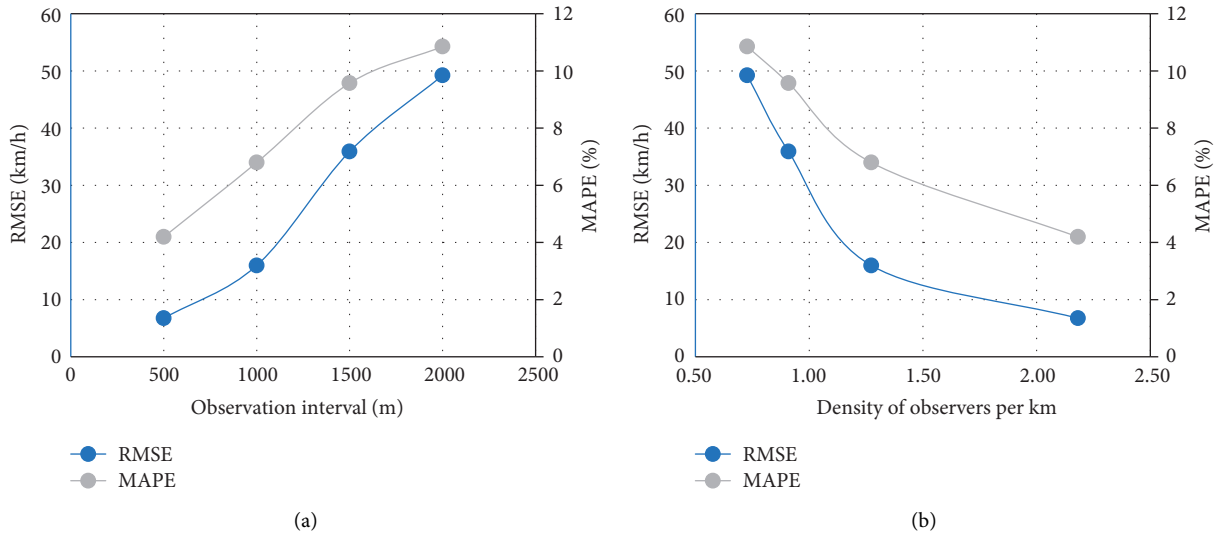

Figure 11: Adaptability of different observation intervals: (a) result under different observation intervals; (b) result under different density of observers.

Table 5: Result of scenarios with missing ramp observers.

Scenario	All cells in the channel						Cell without ramp observers					
	Result			Error			Result			Error		
	RMSE (km/h)	MAE (km/h)	MAPE (%)	RMSE (km/h)	MAE (km/h)	MAPE (%)	RMSE (km/h)	MAE (km/h)	MAPE (%)	RMSE (km/h)	MAE (km/h)	MAPE (%)
CASE C-1	7.59	2.53	4.34	0.86	0.08	0.15	19.54	4.14	5.81	10.34	0.96	1.71
CASE C-2	11.74	3.01	4.81	5.01	0.55	0.62	69.06	10.34	11.62	56.05	6.20	6.87
CASE C-3	51.61	4.17	6.12	44.88	1.72	1.93	501.15	21.44	25.66	495.45	19.17	21.59
CASE C-4	48.50	4.31	6.55	41.77	1.86	2.36	461.33	22.13	29.29	455.62	19.86	25.22
CASE C-5	28.63	3.64	6.22	21.90	1.19	2.03	253.58	16.87	28.71	242.80	13.65	22.95
CASE C-6	28.40	3.66	5.78	21.67	1.21	1.59	228.78	14.12	19.67	224.11	12.10	15.77
CASE C-7	27.79	3.77	6.18	21.06	1.31	1.99	231.52	15.82	24.76	226.84	13.79	20.86
CASE C-8	31.51	3.95	6.56	24.78	1.49	2.37	283.22	19.95	31.91	273.36	16.53	26.24

Moreover, for the same cell (CASE C-6 and CASE C-7, for example), when the ramps' inflow and outflow are relatively similar, the error caused by the absence of the off-ramp's observation equipment is smaller than that caused by the absence of the on-ramp observation equipment. In other words, the impact of the absence of the off-ramp's observation equipment is relatively small. Also, the impact of ramp observer loss on the estimated results is lower than that with 1000m or longer distance interval and is close to that of the road observer damage environment.

6. Conclusion

Under the global development of autonomous driving, the new generation of urban infrastructure is required. However, limited by the financial and investment input, it is quite necessary to model a new traffic flow model which is not only applicable to autonomous driving vehicles but also can adapt to the existing urban observation infrastructure. Therefore, this paper discusses the applicability of the N-X traffic state estimation model in the actual observation environment by

taking the ALPR technology as an example. This manuscript first analyzes the existing problems in the ALPR system's observation environment in practice. Secondly, based on the observation mechanism of vehicle license plate recognition technology, the ALPR observation environment is simulated based on the simulated channel modeling. Finally, through the observation scene design, the ability to adapt to the actual measurement environment is discussed from three aspects: trunk road observation equipment damage, trunk road observation interval distance, and ramp observation equipment missing. The experimental results reveal several key features of the adaptability of the N-X traffic state estimation model in actual observation environment:

(1) The trunk road observation interval has the most significant influence on the estimation results of the N-X traffic state estimation model. The accuracy of the traffic state estimation model can be significantly improved by shortening the distance between adjacent observation devices. In addition, it is found that the accuracy of the estimation results can be improved with the highest efficiency under the premise of limited equipment input by reducing the observation intervals to 1000 m and increasing the density of observer layout to 1 device per kilometer.

(2) The influence of the damage of trunk road observation equipment on the results of n-X traffic state estimation model is less than the influence of excessive interval. When the traffic conditions on both sides of the observation equipment are relatively similar, the damage of the observation equipment has little influence on the traffic state estimation results. However, when the traffic conditions on both sides of the observation equipment are significantly different, the damage of the observation equipment has a great impact on the traffic state estimation results. Therefore, for the section with relatively homogeneous traffic conditions, the layout of observation equipment can be relatively reduced. However, for the road sections with different traffic conditions, the normal operation of observation equipment should be ensured in priority, and the arrangement of observation equipment can be increased relatively.

(3) The impact of ramp metering on the estimated results is smaller than that of the oversize (1.5 km or more) of the observation interval of the trunk road and is close to the damage of the observation equipment of the trunk road. In addition, for ramps with high flow rate, the absence of ramp observation equipment has a relatively small impact on the estimated results. For ramps with low flow rate, the absence of ramp observation equipment will significantly increase the estimation error and reduce the estimation accuracy. In addition, compared with the absence of on-ramp observation equipment, the absence of off-ramp observation equipment has relatively little impact on traffic status estimation results. Therefore, in the case of limited equipment investment, observation equipment should be placed on the on-ramp in priority, and maintenance of observation equipment on the ramp with large flow can be slowed down appropriately.

Future work following this study may include the N-X estimation framework to more complicated automated connected applications in the intelligent transportation system. Furthermore, field probe vehicle data-based estimation analysis is desired to reveal the actual potentials of the proposed model in practice.

Notations

n: The order of the vehicle packet and vehicle coordinate
x: Location, distance on a road, and space coordinate
t: Time, duration, and time coordinate
k: Density, $k = -(\partial n/\partial x)$
q: Flow, $q = (\partial n/\partial t)$
u: Speed, $u = (\partial x/\partial t)$
p: Time headway between two vehicles, $p = (\partial t/\partial n)$ and $p = (1/q)$
τ: Travel time density and travel time over a unit distance, $\tau = (\partial t/\partial x)$ and $\tau = (1/u)$
h: Distance headway between two vehicles, $h = -(\partial x/\partial n)$ and $h = (1/k)$
Δx: Segment length
Δn: Number of vehicles in a flow packet n and packet size
T: Travel time, $T = \tau \times \Delta x = p \times \Delta n$.

Data Availability

The data used to support the findings of this study are available from the corresponding author upon request.

Conflicts of Interest

The authors declare that there are no conflicts of interest regarding the publication of this paper.

Authors' Contributions

Han Yang was responsible for supervision and conceptualization, and Qing Yu carried out writing: review and editing.

Acknowledgments

This paper was supported by Special Funds for Basic Scientific Research Operating Expenses of National Public Research Institutes (grant nos. 2019–0068) and the National Natural Science Foundation of China (grant no. 71734004).

References

[1] J. Levinson, J. Askeland, J. Becker et al., "Towards fully autonomous driving: systems and algorithms," in *Proceedings of the 2011 IEEE Intelligent Vehicles Symposium*, pp. 163–168, Dearborn, MI, USA, 2011.

[2] K. Jo, J. Kim, D. Kim, C. Jang, and M. Sunwoo, "Development of autonomous car-Part II: a case study on the implementation of an autonomous driving system based on distributed architecture," *IEEE Transactions on Industrial Electronics*, vol. 62, no. 8, pp. 5119–5132, 2015.

[3] J. Capus, "POWDERMET2017: the future of electrification and autonomous driving: coming sooner than you think," *Metal Powder Report*, vol. 72, no. 5, pp. 314–316, 2017.

[4] F. van Wageningen-Kessels, H. Van Lint, S. P. Hoogendoorn, and K. Vuik, "Lagrangian formulation of multiclass kinematic wave model," *Transportation Research Record: Journal of the Transportation Research Board*, vol. 2188, no. 1, pp. 29–36, 2010.

[5] L. Leclercq, J. Laval, and E. Chevallier, "The lagrangian coordinate system and what it means for first order traffic flow model," in *Proceedings of the 17th International Symposium on Transportation and Traffic Theory*, New York, USA, 2007.

[6] P. I. Richards, "Shock waves on the highway," *Operations Research*, vol. 4, no. 1, pp. 42–51, 1956.

[7] M. J. Lighthil, "A theory of traffic flow on long crowded roads," *Proceedings of The Royal Society*, vol. 2291178 pages, 1955.

[8] C. F. Daganzo, "The cell transmission model, part II: network traffic," *Transportation Research Part B: Methodological*, vol. 29, no. 2, pp. 79–93, 1995.

[9] C. F. Daganzo, "The cell transmission model: a dynamic representation of highway traffic consistent with the hydrodynamic theory," *Transportation Research Part B: Methodological*, vol. 28, no. 4, pp. 269–287, 1994.

[10] P. J. Jin, K. Han, and B. Ran, "Some theoretical and practical perspectives of the travel time kinematic wave model: generalized solution, applications, and limitations," in *Proceedings of the Transportation Research Board 93rd Annual Meeting*, Washington, DC, USA, 2014.

[11] H. Yang, P. J. Jin, B. Ran, D. Yang, Z. Duan, and L. He, "Freeway traffic state estimation: a Lagrangian-space Kalman filter approach," *Journal of Intelligent Transportation Systems*, vol. 23, no. 6, pp. 525–540, 2019.

[12] H. Yang, J. P. Jin, Z. Duan, B. Ran, D. Yang, and L. He, "Vehicle-space traffic-state estimation of a motorway corridor with slip roads," *Proceedings of the Institution of Civil Engineers - Transport*, vol. 172, no. 1, pp. 47–56, 2019.

[13] Q. Yu, H. Zhang, W. Li et al., "Mobile phone data in urban bicycle-sharing: market-oriented sub-area division and spatial analysis on emission reduction potentials," *Journal of Cleaner Production*, vol. 254, Article ID 119974, 2020.

[14] Q. Yu, H. Zhang, W. Li, X. Song, D. Yang, and R. Shibasaki, "Mobile phone GPS data in urban customized bus: dynamic line design and emission reduction potentials analysis," *Journal of Cleaner Production*, vol. 272, Article ID 122471, 2020.

[15] W. Jiang, H. Zhang, Y. Long et al., "GPS data in urban online ride-hailing: the technical potential analysis of demand prediction model," *Journal of Cleaner Production*, vol. 279, Article ID 123706, 2021.

[16] G. Harrison, S. M. Grant-Muller, and F. C. Hodgson, "New and emerging data forms in transportation planning and policy: opportunities and challenges for "Track and Trace" data," *Transportation Research Part C: Emerging Technologies*, vol. 117, Article ID 102672, 2020.

[17] Q. Yu, W. Li, D. Yang, and Y. Xie, "Policy zoning for efficient land utilization based on spatio-temporal integration between the bicycle-sharing service and the metro transit," *Sustainability*, vol. 13, no. 1, p. 141, 2021.

[18] S. Du, M. Ibrahim, M. Shehata, and W. Badawy, "Automatic license plate recognition (ALPR): a state-of-the-art review," *IEEE Transactions on Circuits and Systems for Video Technology*, vol. 23, no. 2, pp. 311–325, 2012.

[19] Z.-X. Chen, C.-Y. Liu, F.-L. Chang, and G.-Y. Wang, "Automatic license-plate location and recognition based on feature salience," *IEEE Transactions on Vehicular Technology*, vol. 58, no. 7, pp. 3781–3785, 2009.

[20] Y. Wang, P. Coppola, A. Tzimitsi, A. Messmer, M. Papageorgiou, and A. Nuzzolo, "Real-time freeway network traffic surveillance: large-scale field-testing results in southern Italy," *IEEE Transactions on Intelligent Transportation Systems*, vol. 12, no. 2, pp. 548–562, 2011.

[21] Y. Wang, M. Papageorgiou, A. Messmer, P. Coppola, A. Tzimitsi, and A. Nuzzolo, "An adaptive freeway traffic state estimator," *Automatica*, vol. 45, no. 1, pp. 10–24, 2009.

[22] Y. Wang, M. Papageorgiou, and A. Messmer, "Real-time freeway traffic state estimation based on extended Kalman filter: adaptive capabilities and real data testing," *Transportation Research Part A: Policy and Practice*, vol. 42, no. 10, pp. 1340–1358, 2008.

[23] Y. Wang, M. Papageorgiou, and A. Messmer, "Investigation of the adaptive features of a real-time nonlinear freeway traffic state estimator," *Nonlinear Dynamics*, vol. 49, no. 4, pp. 511–524, 2007.

[24] Y. Wang, M. Papageorgiou, and A. Messmer, "Real-time freeway traffic state estimation based on extended Kalman filter: a case study," *Transportation Science*, vol. 41, no. 2, pp. 167–181, 2007.

[25] Y. Wang, M. Papageorgiou, and A. Messmer, "A real-time freeway network traffic surveillance tool," *IEEE Transactions on Control Systems Technology*, vol. 14, no. 1, pp. 18–32, 2005.

[26] Y. Wang, M. Papageorgiou, and A. Messmer, "Renaissance - a unified macroscopic model-based approach to real-time freeway network traffic surveillance," *Transportation Research Part C: Emerging Technologies*, vol. 14, no. 3, pp. 190–212, 2006.

[27] M. Treiber, A. Hennecke, and D. Helbing, "Derivation, properties, and simulation of a gas-kinetic-based, nonlocal traffic model," *Physical Review E*, vol. 59, no. 1, p. 239, 1999.

[28] L. Mihaylova, A. Hegyi, A. Gning, and R. K. Boel, "Parallelized particle and Gaussian sum particle filters for large-scale freeway traffic systems," *IEEE Transactions on Intelligent Transportation Systems*, vol. 13, no. 1, pp. 36–48, 2012.

[29] P. J. Jin and S. D. Boyles, "The Travel Time Transmission model for dynamic network loading," in *Proceedings of the Transportation Research Board 93rd Annual Meeting*, Washington, DC, USA, 2014.